





Measurement of red blood cell deformability during morphological changes using rotating-glass-plate-based scanning optical tweezers

RUI LIU,¹ MENG SHAO,² ZEYU KE,¹ CHANGXU LI,¹ FENGYA LU,¹ MIN-CHENG ZHONG,²  YUXIN MAO,¹ XUNBIN WEI,^{1,3} ZHENSHENG ZHONG,^{1,5} AND JINHUA ZHOU^{1,4,6} 

¹School of Biomedical Engineering, Anhui Medical University, Hefei 230032, China

²School of Instrument Science and Optoelectronics Engineering, Hefei University of Technology, Hefei 230009, China

³Biomedical Engineering Department, Peking University, Beijing 100081, China

⁴3D-Printing and Tissue Engineering Center, Anhui Provincial Institute of Translational Medicine, Anhui Medical University, Hefei 230032, China

⁵zhongzhensheng@ahmu.edu.cn

⁶zhoujinhua@ahmu.edu.cn

Abstract: It is important to measure the deformability of red blood cells (RBCs) before transfusion, which is a key factor in the gas transport ability of RBCs and changes during storage of RBCs *in vitro*. Moreover, the morphology of RBCs also changes during storage. It is proposed that the change in morphology is related to the change in deformability. However, the efficiency of typical methods that use particles as handles is low, especially in the deformability measurement of echinocyte and spherocytes. Therefore, the deformability of RBCs with different morphologies is hard to be measured and compared in the same experiment. In this study, we developed a cost-effective and efficient rotating-glass-plate-based scanning optical tweezers device for the measurement of deformability of RBCs. The performance of this device was evaluated, and the deformability of three types of RBCs was measured using this device. Our results clearly show that the change of erythrocyte morphology from discocyte to echinocyte and spherocyte during storage *in vitro* is accompanied by a decrease in deformability.

© 2023 Optica Publishing Group under the terms of the [Optica Open Access Publishing Agreement](#)

1. Introduction

The principle therapy of hemorrhagic shock after injury is transfusion [1]. In clinical practice, most of red blood cells (RBCs) needed for transfusion are derived from cryogenic bagged blood in the blood bank. However, due to oxidative stress [2] and ATP depletion [3], damage of RBCs is caused over time during storage *in vitro* [4]. During the storage of RBCs *in vitro*, the stiffness of the erythrocyte membrane is gradually increasing [5], and the shape of RBCs also changes from discocyte to spherocyte [6,7]. Deformability is a key factor of the oxygen and carbon dioxide transport ability of RBCs in the capillaries, which is closely related to the stiffness and viscosity of RBCs [8]. Within 24 hours, only 0.8% of the RBCs are removed in healthy people., which mainly happen in the spleen [9,10]. When transfused with blood stored for six weeks, however, that ratio rises to 25% [11,12]. In the red pulp of spleen, in order to reenter the venous system, RBCs must cross the narrow interendothelial slits in walls of the venous sinuses, which requires erythrocytes to undergo remarkable deformation [13,14]. Moreover, the increased stiffness of RBCs induces phagocyte to clear RBCs [15,16]. As a result, the RBCs with larger stiffness are more likely to be trapped and cleared in the spleen [17,18]. Therefore, it may be failed to

replenish enough RBCs if the blood for transfusion has high population of poorly deformable RBCs. Therefore, evaluation of deformability of RBCs is very important for clinical transfusion.

Currently, methods such as automated rheoscopy [19], micropipette aspiration [20,21], microfluidic [5,22], quantitative phase microscopy [23,24] and microfiltration [25] had been used to detect the deformability of RBCs. By exerting force accurately in the order of piconewton on transparent beads or cells without direct contact, optical tweezers have also been applied to manipulate RBCs [26–31].

There are many methods have been applied to detect the RBC deformability using optical tweezers in previous studies. In the single-handle method, [32] one end of an RBC is attached to a polystyrene or silica particle, and the other end is attached to the bottom surface of the chamber. In this method, the area of the RBC attached to the bottom is uncertain, which results in a large measurement uncertainty of elastic modulus. To reduce such uncertainty, in the dual-handle method, one more particle are placed in between the RBC and the bottom surface [33]. Though the elastic modulus of RBCs can be measured accurately using this method, it is difficult to attach two particles to echinocyte or spherocyte effectively, resulting in low measurement efficiency. Combining microfluidics with optical tweezers, [34] the deformability of RBCs can be measured effectively by exerting both optical force and hydrodynamic force. However, the stretching of the spherocyte can be realized only when the flow velocity in the microfluidic chip is high enough, which requires a high frame-rate camera to accurately measure the deformation of the RBCs. Methods that combining optical tweezers with other techniques, such as dielectrophoresis, have also been used to measure the deformability of RBCs [35]. By using dual-fiber optical tweezers combined with microfluidic technology [36,37], high-throughput detection of spherocyte deformability can be achieved by controlling the relative movement by the power of the laser and the distance between the dual-beam optical traps. Furthermore, this technology allows sorting and counting cells based on their properties. However, alignment of two beams from optical fibers needs to manipulate accurately, or it will cause the cells to twist. On the other hand, by using dual-trap optical tweezers with beam scanning device, direct measurement the deformability of RBCs can be achieved via dynamic scanning of optical traps without the aid of microparticle handles, microfluidics, or precise control of position of dual optical traps [38–40]. However, the cost of the beam scanning devices is high. Time-sharing multiples optical tweezers can be also realized by controlling the rotation of different thickness of glass plate in the optical path [41,42]. However, the few discrete trap spots limit the applications in stretching cells with steerable and continuous manners.

In this manuscript, we propose to continuously change the intersection angle between glass plate and one beam by rotation, which forms a scanning optical trap. When a fixed trap holds a cell, the steerable trap can exert optical forces on the cell for stretching. Using this device, we measured the deformability of discocytes, echinocytes and spherocytes during *in vitro* storage. The results showed that our low-cost device enables high throughput detection of erythrocyte deformability.

2. Methods

2.1. Principle of beam scanning

The detailed principle of manipulation of two optical traps using rotating glass plate was described by Jianguang Wu *et al* [41]. When a light ray tilts into the glass plate, the light ray is refracted twice, and the outgoing light ray is parallel to the incident one, with a position offset x between them, as shown in Fig. 1(a). When a slightly divergent beam is emitted from point A, the situation after refraction through the slide is shown in Fig. 1(b), Both slightly divergent beams undergo translation after entering the glass plate, and the offsets of the two rays are denoted as x_+ and x_- , respectively. However, the intersection of the reverse extension of the two outgoing light lines, which is denoted as point B in Fig. 1(b), does not coincide with point A. The offsets of

intersection B relative to the point A in x direction can be expressed as Δx . then the transverse deviations δx in the focal plane of the objective lens satisfies the following equation:

$$\delta x = \frac{\Delta x}{\beta} = \frac{x_+ + x_-}{2\beta \cos \alpha} \approx \frac{x}{\beta} = \frac{t(\sin \theta - \frac{\sin \theta \cos \theta}{\sqrt{n^2 - \sin^2 \theta}})}{\beta}. \quad (1)$$

Where the incident angle of the light is θ , the thickness of the plate is t , and the refractive index of the plate is n , the magnification of the objective lens is β .

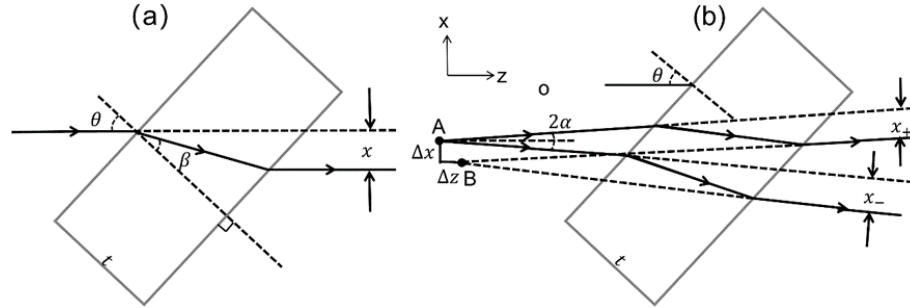


Fig. 1. Schematic representation of the propagation of the light through the glass plate. (a) A single beam of light. (b) A slightly divergent beam.

2.2. Experimental setup

The principle of the optical tweezers system is shown in Fig. 2(a). A dual-beam optical tweezers system was constructed with an inverted optical microscope (Olympus IX73, Japan). In this system, a 1064-nm single-mode fiber laser (Amonics, AFL-1064-37-R-CL, Hong Kong) with maximum output power of 5 W was highly focused to form optical traps, and an electronic shutter was applied to remotely switch the on or off status for optical trap. Through a polarizing beam splitter (PBS), the laser was split into S and P waves. Each beam expansion group consists two K9 plano-convex lens to enlarge the laser diameter to fill the posterior pupil of 60× water immersion objective (NA = 1.2). To achieve dynamic scanning of the P wave, a motor (PUFEIDE, 42BYGH60-401A, China)-driven glass plate (G) is placed behind the focus point of the P wave beam expansion system. Finally, we reassembled the two laser beams by PBS and reflected the laser into the objective lens by a dichroic mirror (DM) to form a dynamic scanning dual-trap optical tweezers system. When the motor-driven glass plate rotates, one of the dual optical traps is offset, while the other remains unchanged. During the stretching experiment, the two optical traps are directly placed to both ends of an RBC. By controlling the rotation of the glass plate, the distance between the two optical traps is gradually increased, so that the RBC is stretched. The process of stretching an RBC using the scanning optical tweezers is illustrated in Fig. 2(b).

2.3. Materials

In this study, a chamber formed by gluing a 22 × 22 mm cover glass and a 25 × 75 mm slide together using hot-melt parafilm, which contains a long rectangular cavity. The chamber was heated at 80 °C for 1 minute to bond the layers. The blood sample from a healthy donor was obtained by venipuncture and stored in blood collection tube (including CPDA-1, proportion of CPDA-1: whole blood = 1.4:10) at 4 ± 2 °C. After storing four weeks, the blood sample was diluted with 1× phosphate buffered saline (Spark Jade, CR0014-500 ML, China, pH 7.4) at 1:400, and then the diluted sample contains all three morphological types of the RBCs [43]. The proportions of discocytes, echinocytes and spherocytes were 26%, 56% and 18%, respectively

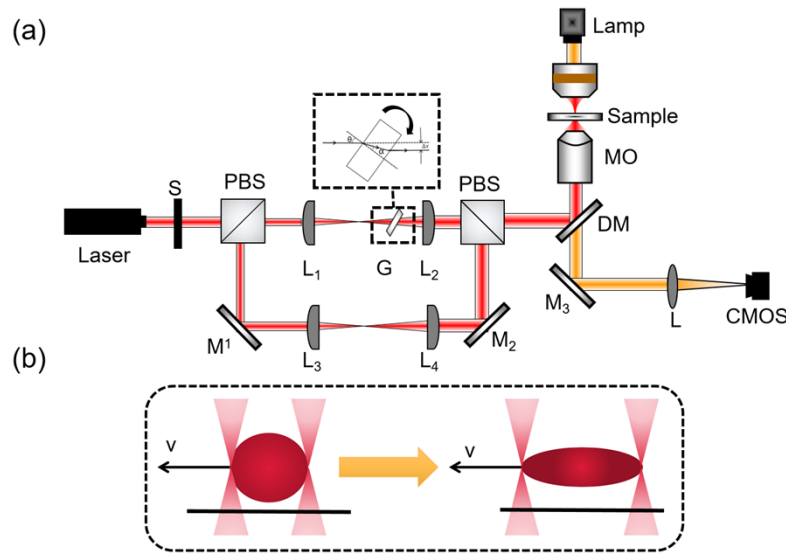


Fig. 2. Schematic diagram of the dynamic scanning optical tweezers device. (a) PBS is polarizing beam splitter. M is mirror, L1 and L2, L3 and L4 constitute 1.67 times the beam expansion system, G is 1 mm thick quartz glass plate, DM is dichroic mirror, and MO is 60X water immersion objective. (b) Schematic representation of the RBCs stretching experiment using the dynamic scanning optical tweezers device.

($N = 602$). To avoid nonspecific adhesion of RBCs to the surface of the chamber, the chamber was incubated with casein (Sigma-Aldrich, C8654) solution of 5 mg/ml for 10 min. We placed the sample chamber at an oblique position, and then dropped 60 μ l of diluted RBCs solution at the entrance of the sample chamber. Under the capillarity effect, the solution flows into the sample chamber from the entrance. Finally, sellotapes were stuck at both ends of the cavity to reduce water volatilization in the chamber [44].

3. Results and discussion

3.1. Characterization of rotation-angle dependent trap stiffness

We used 5- μ m polystyrene microspheres to characterize the transverse offset of the optical trap. When the rotation angle of the glass plate was 75° , the transverse offset of the optical trap was 7.5 μ m, as shown in Fig. 3(a). According to Eq. (1), the transverse offset of the optical trap increases with the increase of the rotation angle. We measured the relation between the transverse offset of the optical trap and the rotation angle of the glass plate from 0° to 75° . Experimental results (red dots) are shown in Fig. 3(b), which are in accordance with theoretical values (black curve) from Eq. (1). As the transverse offset of the optical trap changes with the rotation angle of the glass plate, the rotation-angle dependent power of the scanning optical trap was measured and calculated using Fresnel's equations for reflection and transmission of P wave, as shown in Fig. 3(c) [45]. The power loss of the optical trap is not significant when the rotation angle of the glass plate is smaller than 60° . When the rotation angle of the glass plate is larger than 60° , the reflectivity of the glass surface rises sharply, which largely increases the power loss of the laser through the glass plate. In addition, a hydrodynamic method based on Stokes' law was used to measure the rotation-angle dependent stiffness of the scanning optical trap [29], as shown in Fig. 3(d). The experimental results show that the optical trap stiffness and laser power

do not change apparently when the rotation angle of the glass plate ranges from 0° to 35° . Thus, when the rotation angle is within this range, the optical trap stiffness is approximately constant.

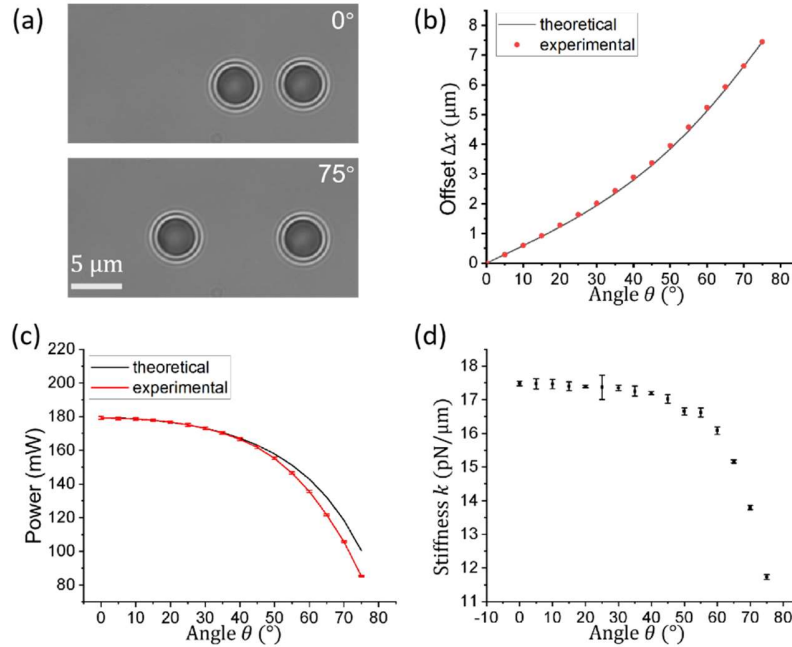


Fig. 3. Characterization of the rotating-glass-plate based scanning optical trap. (a) The transverse offset of optical trap when the glass plate rotation angle is 75° . (b) The relation between the transverse offset of the optical trap and the rotation angle of the glass plate. The black curve is the theoretical value described by Eq. (1). (c) The relation between the power of laser incident on the objective and the rotation angle of the glass plate. The black curve is the theoretical value described by Fresnel's equations for reflection and transmission of P wave. (d) The relation between the stiffness of the optical trap and the rotation angle of the glass plate. Error bars are standard deviations ($N=5$).

3.2. Characterization of force-displacement response ability

To explore the force-displacement response ability of the rotating-glass-plate based scanning optical tweezers device, the motor was rotated in different speeds to drive the plate to oscillate repeatedly within the range of $\pm 35^\circ$, so that the optical trap was reciprocated in the range of $-2.4 \mu\text{m}$ to $+2.4 \mu\text{m}$. Then the force-displacement response curve of the microsphere dragged by the scanning trap was plotted in Fig. 4. The horizontal coordinate shows the oscillating period of the trap. To explore the effect of oscillation response, the interval is 100 ms for periods smaller than 1 s, and 1000 ms for periods larger than 1 s. The vertical coordinate shows the amplitude of displacement of the microspheres dragged by the scanning optical trap, and the dotted line is the amplitude of displacement of the scanning optical trap. When the oscillation period of the trap is smaller than 4 s, the motion displacement response of the microsphere is significantly affected by the viscous resistance. When it is not smaller than 4 s, the displacement response of the microsphere is close to the scanning range of the optical trap, and the response error is not larger than 2.5%. Therefore, when the oscillation period of the trap is 4 s, the influence of viscous resistance on the moving microsphere dragged by the scanning trap is negligible. In this situation, the corresponding moving speed of the scanning trap is $2.4 \mu\text{m/s}$.

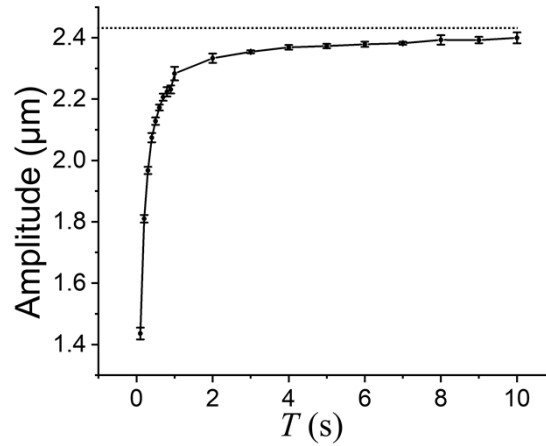


Fig. 4. The force-displacement response of microspheres dragged by the scanning optical trap. Error bars are standard deviations ($N = 5$).

3.3. Measurement of erythrocyte deformability

The distance between the double optical traps is $10\ \mu\text{m}$ when the glass plate rotation angle is 0° . Since the diameter of an RBC is about $5.8\ \mu\text{m}$ to $10.1\ \mu\text{m}$ [46], to ensure each end of an RBC to be trapped by each optical trap, the initial distance between the two optical traps was set to about $4.8\ \mu\text{m}$ to $7.6\ \mu\text{m}$ before capturing the RBC, and the corresponding initial glass plate rotation angle was about -60° to -35° . Before captured by the optical tweezers, the image of the RBC was taken, and the average diameter of the RBC is defined as the original diameter l_0 . Then the glass plate rotated to about 35° , and the corresponding distance between both optical traps changed to about $12.4\ \mu\text{m}$ at a constant speed. During this process, the RBC was stretched to a maximum length just before escaping the scanning trap. The stretching process was recorded by the camera at 90 fps, and the maximum length of the RBC along the stretching direction in the 300-frame video is defined as l_{\max} , then the deformation index DI can be expressed as:

$$DI = \frac{l_{\max} - l_0}{l_0}. \quad (2)$$

By using the rotating-glass-plate based scanning optical tweezers, the deformability of three morphological types of RBCs was measured at the trap moving speed of $2.4\ \mu\text{m/s}$ and the rotation angle of the glass is within $\pm 35^\circ$. As shown in Fig. 5, videos of discocytes, echinocytes and spherocytes before trapping, being captured by the optical tweezers, and escaped from the optical traps were recorded. Then the cellular contour during stretching was analyzed, and the length along the stretching direction was measured.

The Fig. 6(a)–(c) are the estimated kernel density distributions of l_0 and l_{\max} of three types of RBCs. It is clearly that the l_0 of discocytes and echinocytes are close, while that of the spherocytes is significantly smaller, indicating its significant loss of cell membrane. Moreover, the l_{\max} of RBCs significantly reduces with the decline of morphology from discocytes to spherocytes. The Scatter plots of l_{\max} versus l_0 of three types of RBCs are shown in Fig. 6(d)–(f). The scatter plots are fitted using linear regression model through the origin, and the fitting results are $l_{\max}(\text{DC}) = 1.33l_0(\text{DC})$, $l_{\max}(\text{EC}) = 1.23l_0(\text{EC})$, and $l_{\max}(\text{SC}) = 1.18l_0(\text{SC})$ with corresponding R-squared values > 0.999 , respectively. The linear fitting results indicates that the maximum stretched size and initial size of RBCs are positively correlated.

To further characterized the changes of elasticity of RBCs with their decline of morphology, deformability indexes of three types of RBCs were calculated according to the Eq. (2). The

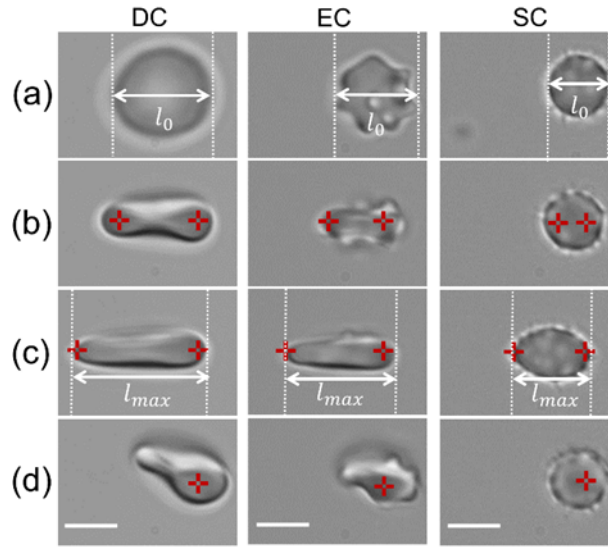


Fig. 5. Schematic representation of stretching of discocytes (DC), echinocytes (EC) and spherocytes (SC) using the scanning optical tweezers. (a) RBCs before stretching. (b) The traps were positioned on the both ends of the RBCs. (c) The RBCs were reached to its maximum length just before escaping from the scanning trap. (d) The relaxed RBCs after escaping from the scanning trap. Here l_0 is the initial diameter of an RBC without stretching, and l_{max} is the maximum length of the same RBC along the stretching direction. The red crosses indicate the centers of optical traps. The length of scale bars is 5 μm .

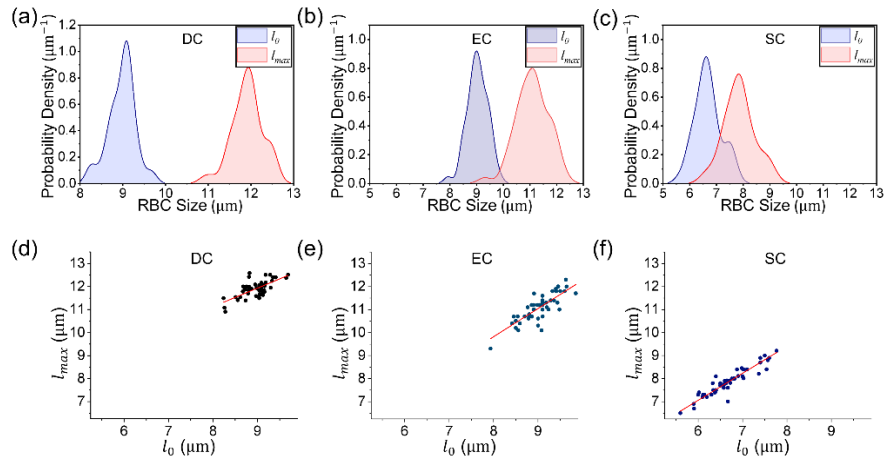


Fig. 6. The initial and maximum stretched sizes of the three types of RBCs. (a-c) Estimated kernel density distributions of l_0 and l_{max} of discocytes (DC), echinocytes (EC) and spherocytes (SC), respectively. (d-f) The scatter plots of l_0 versus l_{max} of the three types of RBCs with corresponding linear fittings through the origin.

distributions of deformability indexes of the three types of RBCs are shown in Fig. 7(a), and Gaussian fittings were applied to the distributions to calculate the 95% confidence intervals of the deformability indexes. The deformability indexes of discocytes, echinocytes and spherocytes were 0.33, 0.23 and 0.18 with corresponding 95% confidence intervals of [0.32, 0.34], [0.22, 0.24] and [0.17, 0.19], respectively. Analysis of Variance (ANOVA) tests indicates that the differences

of deformability indexes among the three types of RBCs are statistically significant, as shown in Fig. 7(b), clearly shown that the deformability of RBCs decreased with the morphology of RBCs changing from discocyte to echinocyte and spherocyte. The scatter plots of the deformability index versus $l_{max}-l_0$ of three types of RBCs are shown in Fig. 7(c), and linear fittings are applied, resulting in $DI(DC) = 0.12(l_{max}(DC) - l_0(DC)) - 0.03$, $DI(EC) = 0.10(l_{max}(EC) - l_0(EC)) + 0.02$, and $DI(SC) = 0.14(l_{max}(SC) - l_0(SC)) + 0.02$ with corresponding R-squared values of 0.89, 0.94 and 0.85, respectively. The scatter plots of deformability index versus the inverse initial RBC size were also fitted linearly (data not shown), resulting in $DI(DC) = \frac{4.61}{l_0(DC)} - 0.19$, $DI(EC) = \frac{0.84}{l_0(EC)} + 0.32$, and $DI(SC) = \frac{0.41}{l_0(SC)} + 0.11$ with corresponding R-squared values of 0.28, 0.01 and 0.02, respectively. The linear regression analysis indicates that the changes of deformability indexes are primarily attributable to the changes of $l_{max}-l_0$, regardless of the initial size of the RBCs. As a result, the decrease of deformability indexes indicates the reduces of elasticity of RBCs with their change of morphology from discocyte to echinocyte and spherocyte.

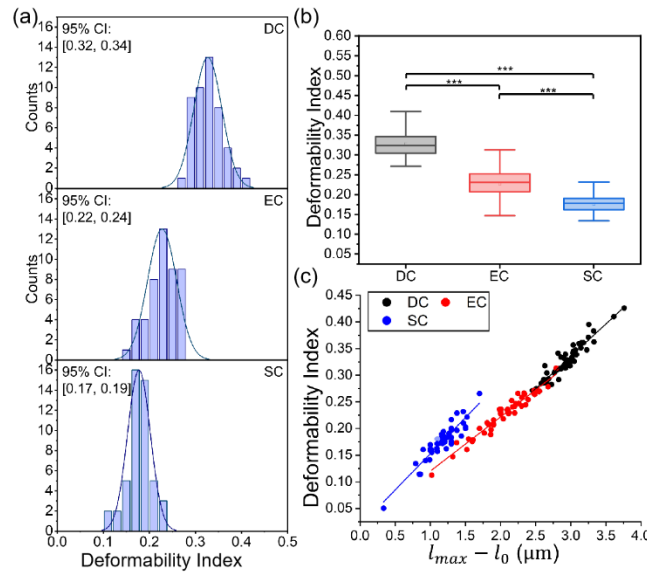


Fig. 7. Results of the deformability of three types of RBCs. (a) Distributions of the deformation index of the three types of RBCs. (b) Boxplot of the deformation index of three types of RBCs. (c) Scatter plots of deformability index versus $l_{max}-l_0$ of the three types of RBCs with corresponding linear fittings. DC, EC and SC are the abbreviations of discocyte, echinocyte and spherocyte, respectively.

The decrease of deformation index with change of morphology of RBCs from discocyte to echinocyte and spherocyte measured in this study, is consistent with the trends that bending modulus, shear modulus and area modulus increase during the morphological change of RBCs [23]. In previous studies, numerical simulations of the deformation characteristics of discocyte and echinocyte were used to predict the minimum shear modulus of echinocyte, which indicates that echinocyte have greater stiffness than discocyte [47]. Such deterioration in RBC quality that occur during in vitro storage of RBCs are collectively referred to as “storage lesion” [48]. It is generally accepted that late echinocytes progressively lose membrane through budding of microvesicles from their spicules [49], and the sphericity of erythrocytes increases during this process, which increased the irreversibility of RBCs morphological changes [50]. Such membrane loss leads to the decrease of deformability observed in this study.

4. Conclusion

In summary, we have successfully applied the cost-effective rotating-glass-plate based scanning optical tweezers device to the measurement of RBCs deformability. By using this device, RBCs can be stretched by two optical traps without the need of attaching microspheres as handles, and high-efficient and high-accuracy measurement of deformability indexes is achieved. We measured the deformability of three morphological types of RBCs, revealing that the deformability indexes decrease with the change of morphology of RBCs from discocyte to echinocyte and spherocyte. Our results indicate the change in morphology of RBCs, which occurs during in vitro storage and is accompanied by loss of membrane, correlates to the loss of deformability. Our device enables fast, accurate and high-throughput measurement of deformability of RBCs, and it is expected to be applied to the detection of mechanical properties of other biological cells in the future.

Funding. Key Research and Development Program of Anhui Province (2022a05020028); Natural Science Foundation of Anhui Province (2208085MC54); Research Fund of Anhui Institute of Translational Medicine (2021zhxy-B16); University Natural Science Research Project of Anhui Province (KJ2021A0252); Key Scientific Research Foundation of Education Department of Anhui Province (2022AH050676).

Disclosures. The authors declare no conflicts of interest.

Data Availability. The data that support the findings of this study are available from the corresponding author upon reasonable request.

References

1. M. Rehn, A. Weaver, K. Brohi, S. Eshelby, L. Green, J. Røislien, and D. J. Lockey, "Effect of prehospital red blood cell transfusion on mortality and time of death in civilian trauma patients," *Shock* **51**(3), 284–288 (2019).
2. B. Küçükakin, V. Kocak, J. Lykkesfeldt, H. J. Nielsen, K. Magnussen, J. Rosenberg, and I. Gögenur, "Storage-induced increase in biomarkers of oxidative stress and inflammation in red blood cell components," *Scand. J. Clin. Lab. Invest.* **71**(4), 299–303 (2011).
3. A. D'Alessandro, A. G. Kriebardis, S. Rinalducci, M. H. Antonelou, K. C. Hansen, I. S. Papassideri, and L. Zolla, "An update on red blood cell storage lesions, as gleaned through biochemistry and omics technologies," *Transfusion* **55**(1), 205–219 (2015).
4. T. Yoshida, M. Prudent, and A. D'Alessandro, "Red blood cell storage lesion: causes and potential clinical consequences," *Blood Transfus.* **17**(1), 27–52 (2019).
5. Z. Xu, Y. Zheng, X. Wang, N. Shehata, C. Wang, and Y. Sun, "Stiffness increase of red blood cells during storage," *Microsyst. Nanoeng.* **4**(1), 17103 (2018).
6. N. Z. Piety, S. C. Gifford, X. Yang, and S. S. Shevkoplyas, "Quantifying morphological heterogeneity: a study of more than 1 000 000 individual stored red blood cells," *Vox Sang.* **109**(3), 221–230 (2015).
7. I. Mustafa, A. Al Marwani, K. Mamdouh Nasr, N. Abdulla Kano, and T. Hadwan, "Time dependent assessment of morphological changes: leukodepleted packed red blood cells stored in SAGM," *Biomed. Res. Int.* **2016**, 4529434 (2016).
8. M. Brandao, A. Fontes, M. Barjas-Castro, L. Barbosa, F. Costa, C. Cesar, and S. Saad, "Optical tweezers for measuring red blood cell elasticity: application to the study of drug response in sickle cell disease," *Eur. J. Haematol.* **70**(4), 207–211 (2003).
9. Y. Gottlieb, O. Topaz, L. A. Cohen, L. D. Yakov, T. Haber, A. Morgenstern, A. Weiss, K. C. Berman, E. Fibach, and E. G. Meyron-Holtz, "Physiologically aged red blood cells undergo erythrophagocytosis in vivo but not in vitro," *Haematologica* **97**(7), 994–1002 (2012).
10. W. H. Crosby, "Normal functions of the spleen relative to red blood cells: a review," *Blood* **14**(4), 399–408 (1959).
11. R. S. Franco, "Measurement of red cell lifespan and aging," *Transfus. Med. Hemother.* **39**(5), 302–307 (2012).
12. D. M. Mock, N. I. Matthews, S. Zhu, R. G. Strauss, R. L. Schmidt, D. Nalbant, G. A. Cress, and J. A. Widness, "Red blood cell (RBC) survival determined in humans using RBCs labeled at multiple biotin densities," *Transfusion* **51**(5), 1047–1057 (2011).
13. M. F. Cesta, "Normal structure, function, and histology of the spleen," *Toxicol. Pathol.* **34**(5), 455–465 (2006).
14. R. E. Mebius and G. Kraal, "Structure and function of the spleen," *Nat. Rev. Immunol.* **5**(8), 606–616 (2005).
15. M. H. Fens, G. Storm, R. C. Pelgrim, A. Ultee, A. T. Byrne, C. A. Gaillard, W. W. van Solinge, and R. M. Schiffelers, "Erythrophagocytosis by angiogenic endothelial cells is enhanced by loss of erythrocyte deformability," *Exp. Hematol.* **38**(4), 282–291 (2010).
16. N. G. Sosale, T. Rouhiparkouhi, A. M. Bradshaw, R. Dimova, R. Lipowsky, and D. E. Discher, "Cell rigidity and shape override CD47's "self"-signaling in phagocytosis by hyperactivating myosin-II," *Blood* **125**(3), 542–552 (2015).
17. T. R. Klei, S. M. Meinders, T. K. van den Berg, and R. van Bruggen, "From the cradle to the grave: the role of macrophages in erythropoiesis and erythrophagocytosis," *Front. Immunol.* **8**, 73 (2017).

18. M. Luten, B. Roerdinkholder-Stoelwinder, N. P. Schaap, W. J. de Grip, H. J. Bos, and G. J. Bosman, "Survival of red blood cells after transfusion: a comparison between red cells concentrates of different storage periods," *Transfusion* **48**(7), 1478–1485 (2008).
19. A. Bransky, N. Korin, Y. Nemirovski, and U. Dinnar, "An automated cell analysis sensing system based on a microfabricated rheoscope for the study of red blood cells physiology," *Biosens. Bioelectron.* **22**(2), 165–169 (2006).
20. R. Hochmuth and R. Waugh, "Erythrocyte membrane elasticity and viscosity," *Annu. Rev. Physiol.* **49**(1), 209–219 (1987).
21. N. Borghi and F. Brochard-Wyart, "Tether extrusion from red blood cells: integral proteins unbinding from cytoskeleton," *Biophys. J.* **93**(4), 1369–1379 (2007).
22. V. Srinivasan, V. K. Pamula, and R. B. Fair, "An integrated digital microfluidic lab-on-a-chip for clinical diagnostics on human physiological fluids," *Lab Chip* **4**(4), 310–315 (2004).
23. Y. Park, C. A. Best, K. Badizadegan, R. R. Dasari, M. S. Feld, T. Kuriabova, M. L. Henle, A. J. Levine, and G. Popescu, "Measurement of red blood cell mechanics during morphological changes," *Proc. Natl. Acad. Sci. U. S. A.* **107**(15), 6731–6736 (2010).
24. A. A. Evans, B. Bhaduri, G. Popescu, and A. J. Levine, "Geometric localization of thermal fluctuations in red blood cells," *Proc. Natl. Acad. Sci. U. S. A.* **114**(11), 2865–2870 (2017).
25. H. Reid, A. Barnes, P. Lock, J. Dormandy, and T. Dormandy, "A simple method for measuring erythrocyte deformability," *J. Clin. Pathol.* **29**(9), 855–858 (1976).
26. J. Sleep, D. Wilson, R. Simmons, and W. Gratzer, "Elasticity of the red cell membrane and its relation to hemolytic disorders: an optical tweezers study," *Biophys. J.* **77**(6), 3085–3095 (1999).
27. G. Lenormand, S. Hénon, A. Richert, J. Siméon, and F. Gallet, "Direct measurement of the area expansion and shear moduli of the human red blood cell membrane skeleton," *Biophys. J.* **81**(1), 43–56 (2001).
28. M. Dao, C. T. Lim, and S. Suresh, "Mechanics of the human red blood cell deformed by optical tweezers," *J. Mech. Phys. Solids* **51**(11-12), 2259–2280 (2003).
29. R. M. Simmons, J. T. Finer, S. Chu, and J. A. Spudich, "Quantitative measurements of force and displacement using an optical trap," *Biophys. J.* **70**(4), 1813–1822 (1996).
30. H. Zhang and K.-K. Liu, "Optical tweezers for single cells," *J. R. Soc. Interface.* **5**(24), 671–690 (2008).
31. R. Zhu, T. Avsievich, A. Popov, and I. Meglinski, "Optical tweezers in studies of red blood cells," *Cells* **9**(3), 545 (2020).
32. J. Wu, Y. Li, D. Lu, Z. Liu, Z. Cheng, and L. He, "Measurement of the membrane elasticity of red blood cell with osmotic pressure by optical tweezers," *Cryo Letters* **30**(2), 89–95 (2009).
33. J. Mills, L. Qie, M. Dao, C. Lim, and S. Suresh, "Nonlinear elastic and viscoelastic deformation of the human red blood cell with optical tweezers," *MCB Mol. Cell. Biomech.* **1**(3), 169–180 (2004).
34. Z. Yao, C. C. Kwan, and A. W. Poon, "An optofluidic "tweeze-and-drag" cell stretcher in a microfluidic channel," *Lab Chip* **20**(3), 601–613 (2020).
35. M. M. Haque, M. G. Moisescu, S. Valkai, A. Der, and T. Savopol, "Stretching of red blood cells using an electro-optics trap," *Biomed. Opt. Express* **6**(1), 118–123 (2015).
36. J. M. Mauritz, T. Tiffert, R. Seear, F. Lautenschläger, A. Esposito, V. L. Lew, J. R. Guck, and C. F. Kaminski, "Detection of Plasmodium falciparum-infected red blood cells by optical stretching," *J. Biomed. Opt.* **15**(3), 030517 (2010).
37. J. Guck, R. Ananthakrishnan, H. Mahmood, T. J. Moon, C. C. Cunningham, and J. Käs, "The optical stretcher: a novel laser tool to micromanipulate cells," *Biophys. J.* **81**(2), 767–784 (2001).
38. R. Agrawal, T. Smart, J. Nobre-Cardoso, C. Richards, R. Bhatnagar, A. Tufail, D. Shima, P. H. Jones, and C. Pavesio, "Assessment of red blood cell deformability in type 2 diabetes mellitus and diabetic retinopathy by dual optical tweezers stretching technique," *Sci. Rep.* **6**(1), 15873 (2016).
39. M. T. Inanc, I. Demirkan, C. Ceylan, A. Ozkan, O. Gundogdu, U. Goreke, U. A. Gurkan, and M. B. Unlu, "Quantifying the influences of radiation therapy on deformability of human red blood cells by dual-beam optical tweezers," *RSC Adv.* **11**(26), 15519–15527 (2021).
40. Y. Liang, G. Liang, Y. Xiang, J. Lamstein, R. Gautam, A. Bezryadina, and Z. Chen, "Manipulation and Assessment of Human Red Blood Cells with Tunable "Tug-of-War" Optical Tweezers," *Phys. Rev. Appl.* **12**(6), 064060 (2019).
41. W. Jian-Guang, R. Yu-Xuan, W. Zi-Qiang, Z. Cheng, and L. Yin-Mei, "Time-Sharing multiple optical traps using rotating glass plate," *Chin. J. Laser* **36**(10), 2751–2756 (2009).
42. W. Jian-Guang, C. Man, L. Huang, and L. Yin-Mei, "Stability of novel time-sharing dual optical tweezers using a rotating tilt glass plate," *Chin. Phys. Lett.* **27**(2), 028703 (2010).
43. M. Jiang, M. Shao, X. Yang, L. He, T. Peng, T. Wang, Z. Ke, Z. Wang, S. Fang, and Y. Mao, "Automatic classification of red blood cell morphology based on quantitative phase imaging," *Int. J. Opt.* **2022**, 1240020 (2022).
44. L. He, M. Shao, X. Yang, L. Si, M. Jiang, T. Wang, Z. Ke, T. Peng, S. Fang, and S. Zhang, "Morphology analysis of unlabeled red blood cells based on quantitative differential phase contrast microscopy," *Cytometry, Part A* **101**(8), 648–657 (2022).
45. K. K. Sharma, *Optics: Principles and Applications* (Elsevier, 2006).
46. Y. Fung, W. C. Tsang, and P. Patitucci, "High-resolution data on the geometry of red blood cells," *Biorheology* **18**(3-6), 369–385 (1981).

47. N. M. Geekiyanage, E. Sauret, S. C. Saha, R. L. Flower, and Y. T. Gu, "Deformation behaviour of stomatocyte, discocyte and echinocyte red blood cell morphologies during optical tweezers stretching," *Biomech. Model. Mechanobiol.* **19**(5), 1827–1843 (2020).
48. R. Almizraq, J. D. Tchir, J. L. Holovati, and J. P. Acker, "Storage of red blood cells affects membrane composition, microvesiculation, and in vitro quality," *Biomech. Model. Mechanobiol.* **53**(10), 2258–2267 (2013).
49. J. Laczko, M. Szabolcs, and I. Jona, "Vesicle release from erythrocytes during storage and failure of rejuvenation to restore cell morphology," *Haematologica* **18**(4), 233–248 (1985).
50. N. Geekiyanage, E. Sauret, S. Saha, R. Flower, and Y. Gu, "Modelling of red blood cell morphological and deformability changes during in-vitro storage," *Appl. Sci.* **10**(9), 3209 (2020).